ChemistrySelect

Research Article
doi.org/10.1002/slct.202502316

Chemistry Europe
European Chemical Societies Publishing

www.chemistryselect.org

Spondias Tuberosa Seeds as Lignocellulosic Bioadsorbent for Efficient PB (II) Removal: Characterization, Adsorption Modeling, Selectivity, and Reusability

Aliane Cristiane de Sousa Formiga,[a] Isaac Moura Araújo,[a] José Augusto Soares de Araujo,[a] Henrique Douglas Melo Coutinho,*[a] Francisco José de Paula Filho,[b] Yannice Tatiane da Costa Santos,[c] Jorge Marcell Coelho Menezes,[b] and Raimundo Nonato Pereira Teixeira[a]

The objective of this research was to investigate the efficiency of *Spondias tuberosa* seeds (SST) as a bioadsorbent for Pb (II) ions in aqueous solutions. Adsorption isotherms and kinetics as well thermodynamics were studied in a batch system. The SST residue was collected from pulp manufacturing industries in the Cariri region of Ceará, specifically in the city of Juazeiro do Norte, Ceará, Brazil. For the characterization of the adsorbent material, point of zero charge (PZC), scanning electron microscopy (SEM), and infrared spectroscopy (FTIR) analyses were performed. The pHPZC obtained had an average value of 5.3, which was adjusted to 5.5. SEM images revealed the presence of roughness and porosity typical of fibrous plant materials. With increased magnification, the material showed varying pore shapes and sizes, generally derived from the structure of the plant cell wall of the precursor biomass. It was also observed that the adsorption rate reached equilibrium within 30 min. Thus, it was concluded that the SST bioadsorbent demonstrated satisfactory performance in the adsorption of Pb (II) ions with a maximum adsorption capacity of 46.0 mg. g^{-1}. These findings support the use of SST as an environmentally friendly low-cost and efficient biosorbent contributing to sustainable strategies for toxic metals remediation.

1. Introduction

Industrial activity generates a significant volume of waste which, when present in liquid form is referred to as effluent, resulting from the utilization of water and other materials in the production of specific products. When discharged untreated, these effluents have the potential to cause substantial environmental impacts.

Industrial process residues containing toxic metals, when released into water bodies or onto soil surfaces, contribute to the generation of serious environmental problems due to their persistent nature. Due to their chronic toxicity, nonbiodegradability, and environmental bioaccumulation, toxic metals are highly harmful environmental pollutants, affecting water, soil, and marine life.[1] The toxic action of these metals can also lead to death or bioaccumulation, which amplifies the harmful effects of these substances through the food chain.

Lead, mercury, cadmium, chromium, copper, and arsenic are examples of toxic and carcinogenic metals that may be present in effluents. These metals are not easily eliminated from the human body, leading to diseases or poisoning (Lesmana, 2009[2]).

Effluents from industries such as ceramics, paints, plastics, pesticides, automobiles, cement, steel, and batteries[3,4] are rich in lead (II) ions, a toxic pollutant. The release of Pb (II) can significantly increase its concentration in the environment and persist for long periods, resulting in severe health effects. Soluble or moderately soluble lead salts readily enter biological systems through polluted water and soil sources, significantly impacting living organisms. Pb (II) severely affects photosynthesis, water management, nitrogen metabolism, and cell division in plants.[4]

To prevent serious environmental and public health issues, it is necessary to treat generated effluents before discharging them untreated, thereby helping to minimize the concentration of these components in compliance with current legislation.

To protect environmental safety and public health, various treatment methods have been developed and explored across a wide range of environmental and health research areas. Each technology comes with its advantages and disadvantages. Among the most efficient and safe techniques available for the elimination of heavy metals are ion exchange, coagulation, adsorption, membrane filtration, electrodialysis, photo-

[a] *A. C. de S. Formiga, I. M. Araújo, J. A. S. de Araujo, H. D. M. Coutinho, R. N. P. Teixeira*
Department of Biological Chemistry, Regional University of Cariri, R. Cel. Antonio Luis 1161, Crato, Ceará 63105000, Brazil
E-mail: hdmcoutinho@urca.br

[b] *F. J. de P. Filho, J. M. C. Menezes*
Science and Technology Center, Federal University of Cariri, Av. Ten. Raimundo Rocha, 1639, Juazeiro do Norte, Ceará 63048-080, Brazil

[c] *Y. T. da C. Santos*
Federal Institute of Education, Science and Technology of Ceará – campus Juazeiro do Norte, Av. Placido Aderaldo Castelo, 1646, Juazeiro do Norte, Ceara 63.040-540, Brazil

© *2025 The Author(s).* ChemistrySelect *published by Wiley-VCH GmbH.. This is an open access article under the terms of the Creative Commons Attribution License, which permits use, distribution and reproduction in any medium, provided the original work is properly cited.*

© 2025 The Author(s). *ChemistrySelect* published by Wiley-VCH GmbH.

catalysis, microbial systems, electrochemical processes, biological treatment, advanced oxidation processes, and membrane bioreactors.[5] Although effective, some of these methods may have limitations, such as high costs, complexity, time demands, and the generation of residual waste.

One of the effective alternatives for the removal of toxic metals such as Lead (II) from wastewater is the technique of biosorption. This process is a reliable and cost-effective method, characterized by low operational costs, minimal scaling issues, and greater economy in the removal of toxic metals from effluents. Additionally, the adsorption technique is easy to use, flexible, simple in design, and does not produce toxic pollutants (Demirbas, 2008[5]).

Therefore, it is important to employ environmentally friendly methods, such as adsorption to remove Pb (II) from effluents and ensure a healthy environment.[6,7] Adsorption is a green process that has been gaining prominence due to its numerous advantages, including versatility, cost-effectiveness,[8] reduced generation of by-products, biodegradability,[9] and superior efficiency compared to other purification techniques that rely on expensive synthetic and organic compounds.[8–10]

Agricultural waste biomass, such as cashew nut shell,[11] Caryocar coriaceum Wittm shell,[12] raw neem,[13] *Azadirachta indica* A. Juss. seeds,[13] bell pepper seeds,[14] coriander seeds,[15] among others have shown effectiveness in the removal of Pb (II) from wastewater.

Although several studies have investigated the adsorption of Pb (II) ions using different bioadsorbents, the novel use of *Spondias tuberosa* (umbu) seeds represents a significant advancement in the search for alternative, sustainable, and low-cost materials for the treatment of water contaminated with heavy metals. This biomass still scarcely explored scientifically is abundant in the semi-arid regions of Brazil and is often discarded as agro-industrial waste. By investigating its adsorptive potential, this study not only contributes to the valorization of a regional byproduct but also expands the portfolio of promising materials for environmental remediation. The originality of the raw material used adds innovation to the research and reinforces its importance in the context of the circular economy and the development of environmentally friendly technologies.

This study aimed to evaluate the potential of agro-industrial residues for the removal of toxic metals from effluents by investigating the adsorption performance of raw biomass derived from *Spondias tuberosa* seeds (SST). The material was proposed as a novel and sustainable bioadsorbent for the removal or reduction of lead (II) ions present in synthetic effluents, through batch adsorption experiments encompassing kinetic, isothermal, and thermodynamic analyses.

2. Materials and Methods

2.1. Collection and Preparation of Adsorbents

The SST residues were collected from a pulp manufacturing industry located in the Cariri region of Ceará, specifically in the city of Juazeiro do Norte, Ceará, Brazil. After collection, the materials were washed with water 2 to 3 times to remove any remaining pulp, and then exposed to sunlight for natural drying over a period of 3 days.

After the natural drying process, all the material was sent to the Chemistry Laboratory of the Regional University of Cariri, where it initially underwent three cycles of grinding in a forage cutter to achieve a finer appearance. Subsequently, the sieving process was carried out, leaving all the particulate material with a 32-mesh particle fraction.

Once the particulate material was prepared, it was dried in an oven at 60 °C to remove all moisture for further use.

2.2. Material Characterization

2.2.1. Point of Zero Charge (pH_{PZC})

The determination of the pH_{PZC} of the adsorbents is an essential factor in characterizing the material, as it helps indicate the optimal pH range for the adsorption of the target material.The pH_{PZC} represents the pH at which the surface of the adsorbent material remains electrically neutral or at zero charge; thus, adsorbents in contact with solutions with a pH above the pH_{PZC} exhibit a negatively charged surface, while below this point, the surface becomes positively charged (Menk et al., 2019).

The point of zero charge (pH_{PZC}) was determined based on the method adapted from Regalbuto and Robles.[16] Thirteen solutions with initial pH values ranging from 1 to 13 were prepared and 20 mL of each solution was transferred into a 125 mL Erlenmeyer flask containing 0.1 g of the adsorbent, previously weighed using an analytical balance. The flasks were then agitated at 150 rpm using a Nova Ética shaker, model 109–1, for a period of 2 h. After the contact time, the final pH of each solution was measured.

The pH_{PZC} was determined by plotting ΔpH ($pH_{initial} - pH_{final}$) versus $pH_{initial}$, where the intersection point of the curve with the x-axis corresponds to the pH_{PZC}.[17–19]

2.2.2. Scanning Electron Microscopy (SEM)

Electron microscopy is used when information about the morphology of a given material is needed. It is a procedure in which a beam of electrons scans the surface of the material being studied, generating a 3D image.[20]

Knowing that the shape, distribution, and size of pores on the surface of bioadsorbents are directly related to adsorption efficiency—since they influence the direct access of solute molecules to adsorption sites—understanding these parameters through 3D imaging indicates the quality of the material for the process.[21]

The SEM analyses were performed using an SU3500 microscope (Hitachi, Tokyo, Japan) at the Regional University of Cariri (URCA). The SST seed samples were mounted on an aluminum sample holder using carbon tape. The images were acquired under low vacuum (microscope chamber pressure at 100 Pa) with a working distance of 10 mm using a backscattered elec-

© 2025 The Author(s). *ChemistrySelect* published by Wiley-VCH GmbH.

tron detector (BSE) in compositional mode and an electron acceleration voltage of 15 kV.

2.2.3. Fourier Transform Infrared Spectroscopy (FTIR)

The FTIR spectra were obtained in transmittance mode using an Agilent Cary 630 FTIR spectrometer. Fourier transform infrared spectroscopy (ATR-FTIR) in the infrared region was performed using the range of 4000–650 cmiha^{-1}. The data were acquired using Microlab and Resolution Pro software both from Agilent (Santa Clara, USA). The maximum spectral resolution was 2 cm^{-1}, and the presented spectrum corresponds to the average of up to eight readings for each wavenumber.

2.3. Batch Adsorption Experiments

2.3.1. Adsorption Kinetics

The study of adsorption kinetics is important to determine the time at which the samples will reach equilibrium.

The experiment was conducted at the LEAS–Environmental and Sanitary Engineering Laboratory of IFCE, Juazeiro do Norte at the local temperature of 25 °C in duplicates using 10 mL aliquots of lead (II) nitrate solution buffered with acetic solution at 102 mg·L^{-1}, obtaining a concentration in the pH range of 5.5. The solution was transferred to a 125 mL Erlenmeyer flask containing 0.05 g of the weighed adsorbent and then placed on a shaker table at 150 rpm for periods of 1, 4, 8, 16, 30, 60, 120, and 240 min.

After the established contact times were reached, the samples were filtered through filter paper, stored, and transported to the Analytical Center Laboratory of UFCA, where they were analyzed by Flame Atomic Absorption Spectroscopy (FAAS) using a Varian SpectrAA 50B spectrometer.

The experimental results were determined by the adsorptive capacity of the material following the study equations below: Lead (II) adsorption efficiency was determined by Equation (1).

$$E\,(\%) = \frac{(C_0 - C_f)}{C_0} \times 100 \tag{1}$$

where C_0 is the initial ion concentration in the solution (mg·L^{-1}) and C_f is the ion concentration in the solution at time t (mg·L^{-1}).

To fit the data and analyze the metal adsorption rate, linear models of pseudo-first-order kinetics Equation (2), pseudo-second-order kinetics Equation (3), and the Elovich kinetic equation Equation (4) were used.

$$qt = qe \times \left(1 - e^{-k1 \times t}\right) \tag{2}$$

$$qt = \frac{qe^2 \times k_2 \times t}{1 + qe \times k_2 \times t} \tag{3}$$

$$qt = \frac{1}{\beta} \ln\left(1 + \alpha\beta t\right) \tag{4}$$

where qt and qe represent the adsorption capacity at any time and at equilibrium, respectively, in (mg·g^{-1}); k_1 is the pseudo-first-order adsorption rate constant (min^{-1}); k_2 is the pseudo-second-order adsorption rate constant (g·mg^{-1}·min^{-1}); α is the initial adsorption rate (mg·g^{-1}·min^{-1}), and β is the adsorption constant (mg·g^{-1}).

To identify the actual rate-limiting step in the adsorption separations, the intraparticle diffusion kinetic model (5) and the Boyd Equations (6) and (7) were applied.

$$qt = K_d * t^{0,5} + C \tag{5}$$

where qt is the amount of metal adsorbed in the solid phase (mg·g^{-1}) at time t (min); K_d is the intraparticle diffusion coefficient (mg·g^{-1}·min^{0,5}) obtained from the slope and C is the intercept of the qt vs. t^{0,5} graph, representing the constant related to diffusion resistance (mg·g^{-1}).

$$F < 0,85 : Bt = \left(\sqrt{\pi} - \sqrt{(\pi - (\frac{\pi^2 F}{3})}\right)^2 \tag{6}$$

$$F > 0.85 : Bt = -0.49770 - \ln(1 - F)$$

$$B = \frac{\pi^2 D}{r^2} \tag{7}$$

where F is the ratio qt/qe; Bt is the mathematical function of F; D is the effective diffusion coefficient (cm^2·min^{-1}); r is the particle radius (cm); and B is the Boyd model constant (slope).

2.3.2. Adsorption Isotherm

The adsorption isotherms were determined to evaluate the adsorbent's efficiency. The tests were conducted in duplicates, using 0.05 g of biomass with 10 mL of a lead solution at a buffered pH of 5.5 with concentrations ranging from 10 to 700 mg.L^{-1} at the equilibrium time established by the kinetic test under agitation at 150 rpm.

As in the kinetic method, after reaching the contact time, the samples were filtered, and the concentrations were subsequently determined by FAAS.

Adsorption isotherm models were applied to the experimental data using the nonlinear equations of Langmuir, Freundlich, Temkin, and Sips, respectively according to the following equations:

$$qe = \frac{q_{max} \times k_L \times cf}{1 + k_L \times cf} \tag{8}$$

$$qe = K_F \times Cf^{\frac{1}{n}} \tag{9}$$

$$qe = \frac{RT}{b} In\left(K_T \times Cf\right) \tag{10}$$

$$qe = \frac{q_{max} \times k_S \times cf^{\beta s}}{1 + k_S \times cf^{\beta s}} \tag{11}$$

© 2025 The Author(s). ChemistrySelect published by Wiley-VCH GmbH.

where *qe* is the adsorption capacity at equilibrium ($mg{\cdot}g^{-1}$), q_{max} is the theoretical monolayer capacity of the adsorbate on the adsorbent ($mg{\cdot}g^{-1}$); *Ce* is the equilibrium ion concentration in the solution ($mg{\cdot}L^{-1}$); K_L is the Langmuir constant directly related to the equilibrium constant ($L{\cdot}mg^{-1}$); K_F is the Freundlich constant ($(mg{\cdot}g^{-1})(L{\cdot}mg^{-1})1/n$); 1/n is the Freundlich adsorption intensity constant; K_T is the Temkin constant ($L{\cdot}mg^{-1}$); K_S is the Sips constant ($L{\cdot}mg^{-1}$); *n* is the surface heterogeneity factor of the adsorbent; *R* is the universal gas constant ($J{\cdot}mol^{-1}{\cdot}K^{-1}$); *T* is the temperature (K); and *b* is the adsorption heat ($J{\cdot}mol^{-1}$).

2.3.3. Adsorption Thermodynamics

The thermodynamic parameters estimated in this study include the standard Gibbs free energy change ($\Delta G°$) which is related to the spontaneity of the adsorption process; the standard entropy change ($\Delta S°$), which is related to the disorder of the system; and the standard enthalpy change ($\Delta H°$), which indicates whether the process absorbs heat (endothermic) or releases heat (exothermic).

To calculate these thermodynamic parameters, three distinct temperatures were used: 25 °C (ambient temperature), 15 °C, and 35 °C.

The calculations for determining the values of $\Delta G°$, $\Delta H°$, and $\Delta S°$ were performed using the following linear equations:

$$\Delta G^{\circ} = \Delta H^{\circ} - T\Delta S^{\circ} \tag{12}$$

$$\Delta G^{\circ} = -RTLn(K) \tag{13}$$

$$Ln\,(K) = \frac{-\Delta H^{\circ}}{RT} + \frac{\Delta S^{\circ}}{R} \tag{14}$$

$$K_g = q_e/C_e \tag{15}$$

$$K_e{}^{0} = 1000.Kg.d \tag{16}$$

3. Results and Discussions

3.1. Material Characterization

3.1.1. Point of Zero Charge (pH_{PZC})

Organic functional groups on the surface of the biosorbent can acquire either a negative or positive charge depending on the pH of the solution. At pH values higher than the pH_{PZC}, the sites will primarily be in the dissociated form and will acquire a negative charge. Conversely, at pH values lower than the pHpzc, these groups will be in the protonated form resulting in a positive charge.

For lead (II) ions (Pb^{2+}), which are cations, it is essential that the adsorbent surface is covered with negatively charged species to promote the electrostatic attraction and removal of this metal.

Figure 1 depicts the graphical representation of the pH_{PZC} of the raw SST bioadsorbent. As shown in the figure, a constant pH range between 5 and 8 is observed with an average final pH of 5.3, which is considered the pH_{PZC} value. This value was adjusted to a pH of 5.5 to enhance the adsorption of more soluble metal ion compounds.

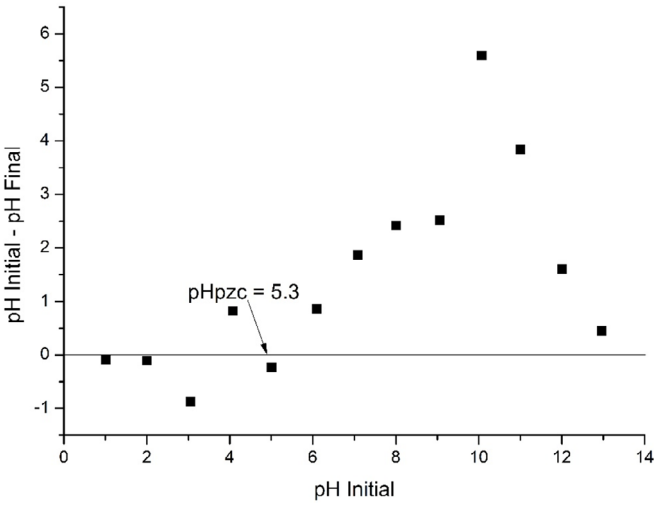


Figure 1. pHpzc of the SST biosorbent.

3.1.2. Scanning Electron Microscopy (SEM)

The images obtained from the scanning electron microscopy (SEM) allow visualization of the morphology of the raw material before and after contact. The micrographs are presented in Figure 2, with magnifications of 75x (A and C) and 500x (B and D), showing the material before and after the adsorption process, respectively.

In the SEM images, the material exhibits roughness and porosity, characteristics typical of fibrous plant materials. With increased magnification, different shapes and sizes of pores become apparent, generally originating from the cell wall structure of the precursor biomass. At 500x magnification, porous spaces with surface irregularities and varying depths of porous channels are clearly visible.

These characteristics are important for characterizing the adsorbent, as they help identify the adsorption process. As highlighted by Barros,[22] the material's surface is highly porous, irregular, and heterogeneous—features that are advantageous for the adsorption of metals in aqueous solutions. Adsorbed components accumulate on the external surface, and a larger surface area per unit mass enhances adsorption.

In Figures 2c,d, a brighter region on parts of the adsorbent's surface is visible, which may indicate the presence of adsorbed Pb (II) ions at those points.

3.1.3. Fourier Transform Infrared Spectroscopy (FTIR)

Through Fourier-transform infrared spectroscopy (FTIR), it was possible to characterize the reactive functional groups present in the material, thereby enabling the investigation of the reaction mechanism involved (Figure 3).[23]

© 2025 The Author(s). *ChemistrySelect* published by Wiley-VCH GmbH.

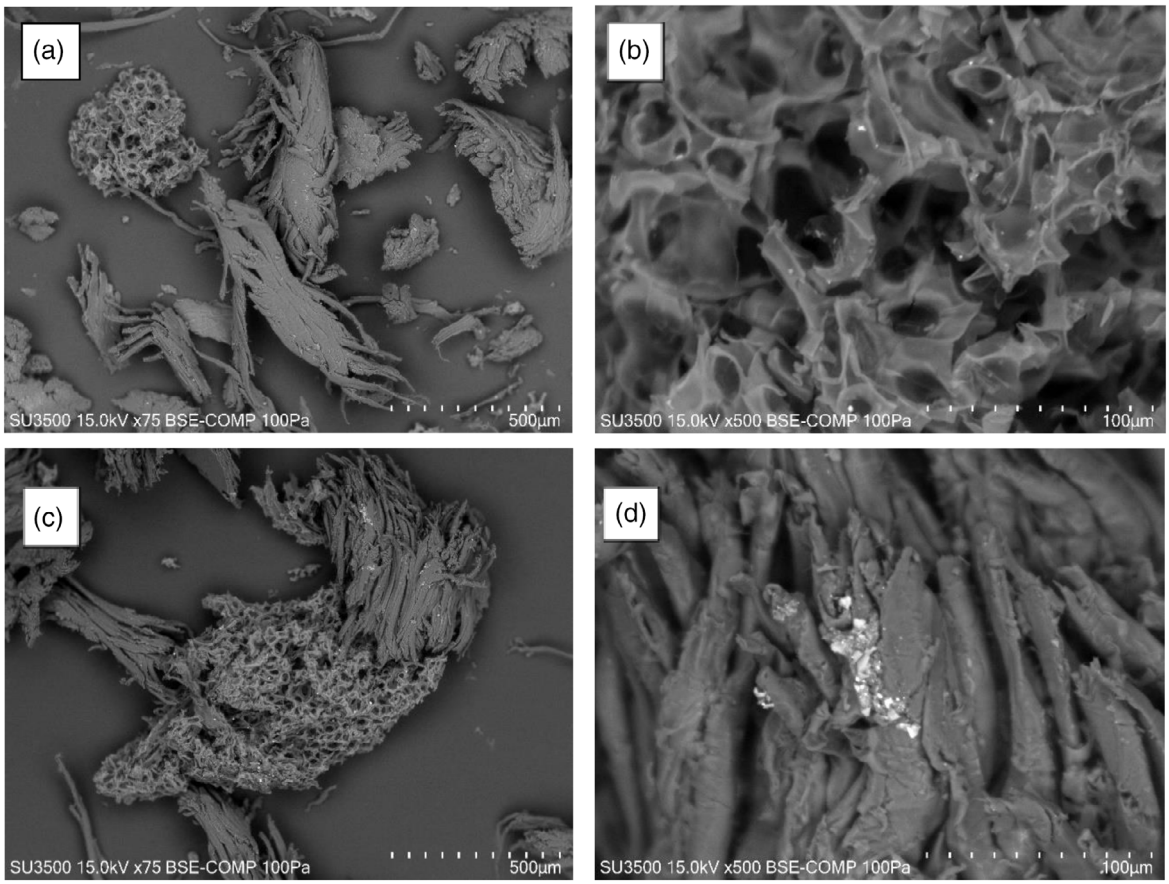


Figure 2. Scanning electron microscopy images of TSM: a) 75x before the adsorption process, b) 500x before the adsorption process, c) 75x after the adsorption process, and d) 500x after the adsorption process.

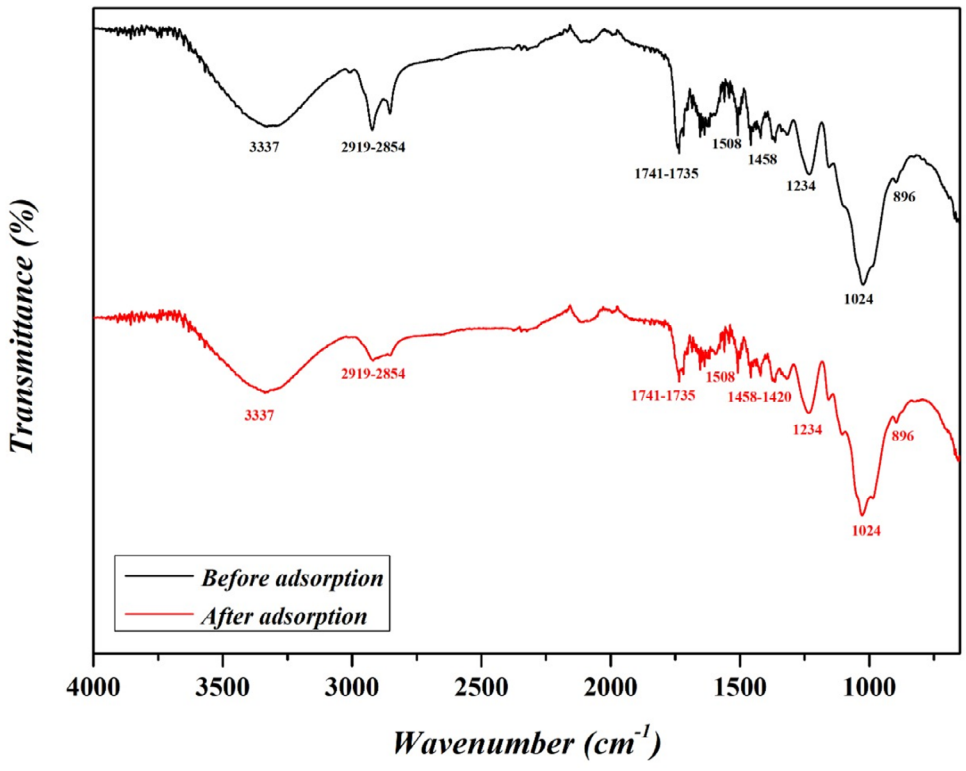


Figure 3. Characterization of raw SST and post contact with Pb (II) ion.

© 2025 The Author(s). *ChemistrySelect* published by Wiley-VCH GmbH.

As observed in Figure 3, the peaks in both spectra at the vibration frequency of 3337 cm^{-1} correspond to O-H and N-H stretching, indicating the presence of hydroxyl groups and amino groups from proteins, fatty acids, carbohydrates, and lignin found in plants. The two smaller peaks at 2919 cm^{-1} and 2854 cm^{-1} correspond to asymmetric C-H vibrations of carbonyl groups and the -OH stretch of carboxylic acids, respectively, relating to the methyl groups in lignin and cellulose. The peaks at 1741–1735 cm^{-1} are associated with C=O stretching vibrations, which, along with the O–H observed at 3337 cm^{-1}, justify the presence of carboxylic acids. The peaks at 1458–1420 cm^{-1} correspond to C–H, indicative of alkanes with bending vibrations that may be related to angular vibrations of $-CH_3$ and $-CH_2-$ groups. A peak at 1234 cm^{-1} represents CO and OH stretching in-plane in polysaccharides.[24]

Thus, through infrared analysis, it is possible to infer that SST exhibits functional groups characteristic of lignocellulosic materials.[25] C=O vibrational bonds in hemicelluloses and extractive compounds such as esterified resin acids, waxes, and fats[26] are present. The lower peaks at 896 and 1024 cm^{-1}, related to CH deformation in cellulose and CO stretching in polysaccharides, fall within the "fingerprint" region and confirm the presence of polysaccharides.[24]

Therefore, the FTIR spectrum characterizes the biomass as lignocellulosic in origin, a component of dried plant material. Lignocellulosic materials composed of cellulose, hemicellulose, and lignin are abundant resources for energy and chemical production.[27]

The presence of hydroxyl (–OH), carboxylic (–COOH), and carbonyl (C=O) groups in the chemical structure of the bioadsorbent significantly contributes to interactions with metal ions. These functional groups contain oxygen atoms with non-bonding electron pairs capable of acting as electron donors, thus facilitating electrostatic attractions, coordination complex formation, or potential ion-exchange mechanisms with Pb (II) ions. The FTIR analysis (Figure 3) revealed notable shifts in the characteristics bands at 2919–2854, 1741–1735, and 1508 cm^{-1}, corresponding precisely to these functional groups, suggesting potential involvement of these functional groups in the adsorption mechanism. Zolgharnein and Farahani[28] further explain that a marked decrease in peak intensity confirms the interaction between metal ions and oxygen atoms, reinforcing the potential of the biomass as a promising material for the removal of toxic metals from aqueous solutions.

3.2. Batch Adsorption Tests

3.2.1. Adsorption Kinetics

The adsorption rate, determined through the adsorption kinetics study, was based on the determination of the adsorptive capacity (qt) of SST in the liquid phase relative to the contact time (t) with the Pb II adsorbate, as represented in the graph shown in Figure 4.

Analyzing Figure 4, it is observed that the adsorption rate reaches equilibrium around 30 min. Initially, the process occurs quite rapidly, but it slows down over time. The curve of the models indicates that even at the early minutes, the adsorptive capacity (qt) shows a significant reduction in the rate of Pb (II) ions. According to Khan,[29] the higher adsorption rate in the initial stages may be due to the greater number of available sites on the adsorbent surface.

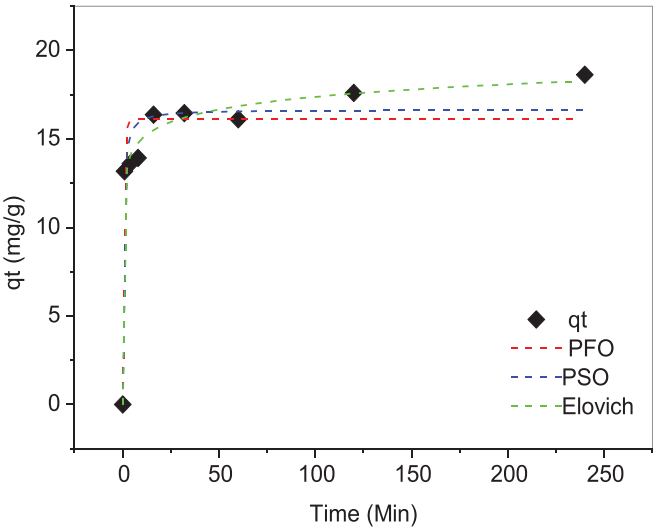


Figure 4. Adsorption kinetics tested for Pb (II) ion removal under test conditions: 25 °C, pH 5.5, 102 mg. L^{-1}, 100 rpm, and 0.05 g of SST adsorbent.

The data in Figure 4 were fitted to the experimental data of pseudo-first-order (PFO) and pseudo-second-order (PSO) adsorption kinetics models, as well as the nonlinear Elovich model. The statistical parameters applied to the nonlinear regression model fittings are presented in Table 1.

According to Figure 4 and the data in Table 1, it is possible to observe a better fit with the Elovich model. Although initially developed for gas adsorption on solid adsorbents, the Elovich model adapts well to studies involving liquid-phase fluids.

The Elovich model demonstrated the best linear regression data and error function, with an R^2 value approaching unity and the lowest SSE and chi^2 errors compared to other models. Additionally, the maximum experimental capacity (q_{max}) and model capacity (q_{model}) values were very close.

The Elovich equation is generally applicable to chemisorption kinetics, as described by Olivares.[30] The Elovich model is based on a general second-order reaction mechanism for the adsorption process, assuming that the adsorbent's active sites are heterogeneous and exhibit varying activation energies for chemisorption.

Thus, comparing the experimental data to the Elovich model reveals that the adsorption process has predominant characteristics of chemisorption. Furthermore, the high α value indicates a high initial adsorption rate and suggests that the attraction of the material occurs via a chemical pathway. The β value, representing the extent of surface coverage and activation energy involved, is low, indicating a rapid adsorption rate with minimal activation energy required for the process.

To determine the rate-limiting step of the adsorption process in the experiment, the Boyd intraparticle model was applied,

© 2025 The Author(s). *ChemistrySelect* published by Wiley-VCH GmbH.

Table 1. Kinetic parameters of the PFO, PSO, and Elovich models using SST as adsorbent.

Models	Parameters							
	q_{model} mg.g^{-1}	q_{max} mg.g^{-1}	R^2 Adjusted	χ^2	SSE	k_1 g.mg^{-1}.min^{-1}	α mg.g^{-1}.min^{-1}	β mg.g^{-1}
PFO	16.1097	18.6	0.9091	2.8093	19.6658	1.6831	–	–
PSO	16.6545	18.6	0.9405	1.8390	12.8729	0.16141	–	–
Elovich	18.2698	18.6	0.9873	0.3919	2.7430	–	2.33069x10^5	0.97508

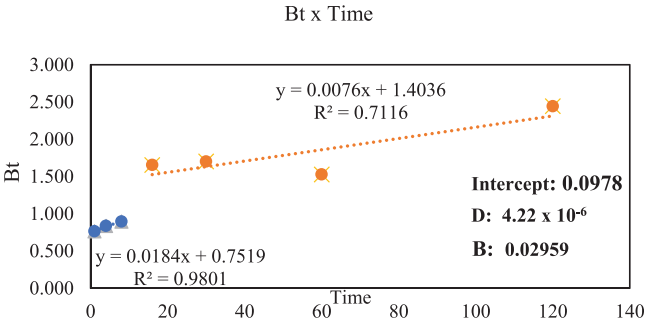


Figure 5. Boyd's Linear Intraparticle Diffusion Model for SST. Where BB is the Boyd model constant (determined by the slope of the straight), D is the coefficient for Boyd's Effective Diffusion in cm^2.min^{-1} and b is the linear coefficient of the straight (intercept).

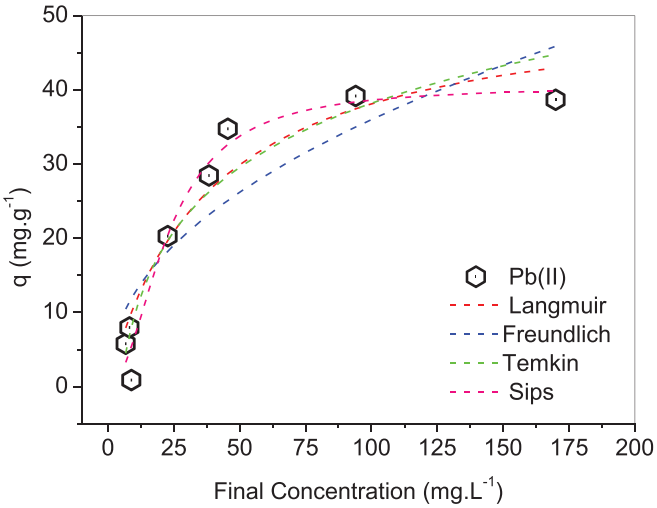


Figure 6. Equilibrium isotherm models of Pb (II) ions to SST adsorbent, until C_0 = 175 mg. L^{-1}. Test conditions: 25 °C, pH 5.5, 60 min, 150 rpm e 0.05 g adsorbent.

resulting in the Bt versus t (min) graph. The Boyd equations described in section 2.3.1 were used to establish the analytical parameters outlined in Figure 5.

According to the data presented, it is observed that the graph does not pass through the origin. Therefore, the Boyd constant is not zero, suggesting that the rate-limiting step of the process is not intra-film diffusion (Yadav, 2023). Additionally, as noted by El-Khaiary and Malash,[31] whether the graph is non-linear or linear, if it does not intersect the origin, the rate-limiting step may be film diffusion or chemical reaction.

With an R^2 value close to unity, the model shows a favorable fit. Furthermore, since the b value of the linear equation of the first line deviates from zero, it is possible that the rate-limiting step is governed by external or intraparticle diffusion, where there is a significant mass transfer of Pb (II) in the SST.

3.2.2. Adsorption Isotherm

The adsorption isotherm was evaluated based on the variation in adsorptive capacity (*qe*) as a function of the equilibrium concentration of the adsorbate (C_e). Figure 6 shows the experimental results for the adsorption of Pb (II) ions compared with the Langmuir, Freundlich, Temkin, and Sips models. According to Figure 6, it is observed that the adsorptive capacity (*qe*) increases with the concentration of the adsorbate (C_e), and equilibrium is reached at a concentration of 100 mg.L^{-1}.

The model that best fit the experimental data was the Sips model, as shown in Figure 6. However, to justify the adsorbent-adsorbate interactions, adsorption mechanisms, and surface-related information, according to Lima[32] the statistical parameters of the isotherms were determined using the linear equations described in section 2.3.2 and are presented in Table 2.

Table 2. Statistical parameters calculated for adsorption isotherms applied to the Langmuir, Freundlich, Temkin and Sips models.

Models	Parameters				
	$q_{max\text{-}experimental}$ (mg.g^{-1})	46.0	R^2 Adjusted	χ^2	SSE
Langmuir	q_{max} (mg·g^{-1})	52.57	0.894	25.4060	152.4
	K_L (L·mg^{-1})	0.02			
Freundlich	K_F (mg·g^{-1}) (L·mg^{-1})$^{1/n}$	4.37	0.758	58.3360	350.0
	1/n	0.45			
	N	2.18			
Temkin	K_T (L·mg^{-1})	0.21	0.903	23.3511	140.1
	b (J/mol)	12.47			
Sips	q_{max} (mg·g^{-1})	40.52	0.960	9.4309	47.1
	K_S (L·mg^{-1})	0.04			
	N	2.02			

The maximum adsorptive capacity determined experimentally was 46.0 mg·g^{-1}, which is consistent with both the Langmuir and Sips models. However, considering the adjusted R^2 value closest to unity and the lower error functions (χ^2 and SSE), the Sips model demonstrates the best fit for the experiment.

In this regard, Aquareles[33] notes that the Sips isotherm has the advantage of being more general than the Langmuir and Freundlich isotherms, as it reduces to each of these models

© 2025 The Author(s). *ChemistrySelect* published by Wiley-VCH GmbH.

Table 3. Lignocellulosic bioadsorbents and maximum adsorption capacities with Pb (II).

Adsorbent	$q_{max,exp}$ (mg.g $^{-1}$)	Reference
Caryocar coriaceum WITTM barks	106.38	[36]
Raw Neem	17.96	[13]
Ziziphus joazeiro barks	58.3	[37]
Azadirachta indica A.Juss Seeds	17.96	[13]
Pepper seeds	48.0	[14]
Coriander seeds	19.76	[15]
Umbu Seed	46.0	This work

under certain limits and can be related to chemical reactions that occur. Thus, the Sips model provides broader insights into the interactions between the adsorbent and adsorbate, elucidating the attractive or repulsive characteristics between them.

Additionally, the Sips model is associated with the energetic heterogeneity of the adsorbent-adsorbate system, which can arise from either the adsorbent, the adsorbate, or their interaction.[34] By analyzing the parameter (*n*) and relating it to heterogeneity, it is observed that when (n) approaches unity (n = 1), it suggests that the system is energetically homogeneous. Conversely, if (n) deviates from 1, the adsorbent-adsorbate system is energetically heterogeneous.[35]

In this case, with (n = 2.02), the system deviated from unity, indicating that it is heterogeneous, which aligns with the infrared data for SST.

According to the experimental data and the Sips mathematical model, it can be inferred that the adsorbent-adsorbate interactions on SST occur heterogeneously, meaning through multilayers, and the system is considered multielemental.

Comparing the adsorption capacity of SST for Pb (II) to other lignocellulosic materials of similar origin, such as biomass from husks and seeds found in the literature, Table 3 highlights SST as an excellent adsorbent for this metal, especially when compared to bioadsorbents derived from seed residuals.

3.2.3. Adsorption Thermodynamics

The thermodynamic study provided insight into the effect of temperature on the adsorption of Pb (II) ions by SST. The thermodynamic parameters (ΔG, ΔH, and ΔS) were determined using the equations described in section 2.3.3, utilizing the equilibrium constant (K_g) from Equation (15), where *qe* is the equilibrium capacity (mg.g^{-1}) and *Ce* is the equilibrium concentration of the metal ions (mg.L^{-1}).

Once the values of K are obtained, a correction must be applied to make the constant dimensionless, as it will be used in the natural logarithm function (Ln) within the van't Hoff equation, which requires a dimensionless input. For this purpose, Equation (16) from Section 2.3.3, as described by Lima et al.,[38] should be used. In this equation: Kg is the constant obtained from the isothermal models (L.mg^{-1}); 1000 is the conversion factor from L.mg^{-1} to L.g^{-1}; and d represents the density of water (1000 g.L^{-1}), assuming that the density of the adsorbate solution is approximately equal to that of water.

Table 4. Thermodynamic Parameters determined from Figure 7b.

Temperature (°C)	$\Delta G°$ (kJ.mol^{-1})	$\Delta H°$ (kJ.mol^{-1})	ΔS (J.mol^{-1}. K^{-1})
15	−36.90		
25	−38.18	7.52	128.15
35	−39.46		

In Figure 7a, an increase in adsorption capacity is observed with rising temperature from 14.1 mg.g^{-1} at 15 °C to 16.36 mg.g^{-1} at 35 °C, indicating a positive enthalpy change ($\Delta H > 0$), confirming the process is endothermic, as presented in Table 4.

As highlighted by Ozsin,[39] the endothermic nature of adsorption can be attributed to the increased mobility of heavy metal ions and an enhanced diffusion rate of adsorbate molecules through the external boundary layer and into the internal pores of the adsorbent, due to a reduction in solution viscosity.

The data presented in Table 4 were obtained using the slope and intercept values from the linear regression line shown in Figure 7b. As indicated by the results, Gibbs free energy ($\Delta G°$) decreases with increasing temperature and assumes negative values, indicating the spontaneous nature of the process. Notably, the process becomes more thermodynamically favorable as the standard Gibbs free energy becomes more negative with increasing temperature, regardless of the nature of the adsorbent, suggesting enhanced efficiency in the adsorption of Pb (II) at lower temperatures.[40,41] Furthermore, the positive value of ΔSads indicates an increase in entropy at the solid–liquid interface, suggesting structural changes in both the adsorbate and the adsorbent,[42] which is consistent with the findings from the FTIR analysis.

The nature of the adsorption process can be either chemical or physical, depending on the interactions between the binding sites. According to Azadian,[43] negative $\Delta G°$ values suggest a physisorption mechanism. Additionally, Hasanzadeh et al.[44] highlight that enthalpy values below 40 kJ.mol^{-1} indicate that the process does not require activation energy, as physical adsorption involves attractive forces between the adsorbent and the adsorbate. In this context, since the experimental process was spontaneous—with a decrease in the system's free energy—and involved heat absorption (endothermic, $\Delta H° > 0$) with enthalpy values below 40 kJ.mol^{-1}, the adsorption mechanism reveals characteristics of physisorption.

4. Conclusion

The present study demonstrated that SST biomass is an effective bioadsorbent for the removal of lead Pb (II) ions from aqueous solutions. Based on batch adsorption experiments, the material reached a maximum adsorption capacity of 46.0 mg·g^{-1}. When compared to other bioadsorbents reported in the literature, SST

© 2025 The Author(s). *ChemistrySelect* published by Wiley-VCH GmbH.

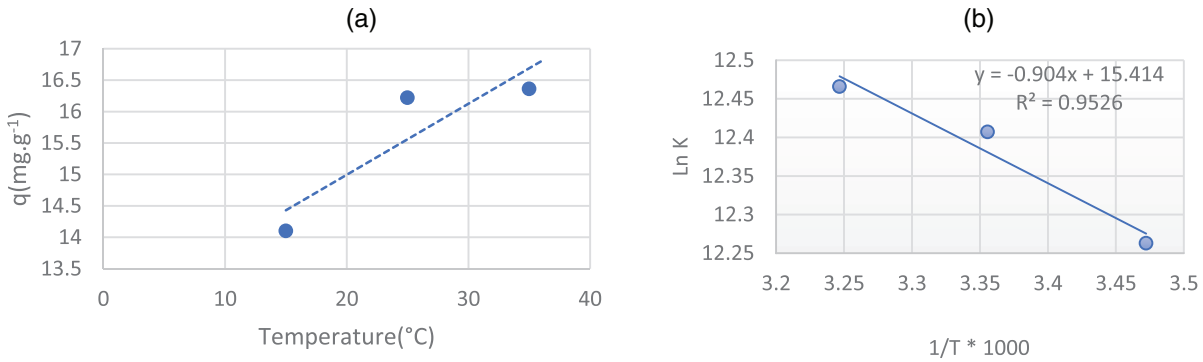


Figure 7. Linear modeling for the determination of ΔG, ΔH, and ΔS for Pb (II) ions in contact with SST under the conditions of 15 °C, 25 °C, and 35 °C, at 60 min, 150 rpm, and pH 5.5.

biomass showed competitive efficiency particularly among seed-derived lignocellulosic materials.

Structural characterization by FTIR and SEM confirmed the lignocellulosic nature of the adsorbent, revealing the presence of cellulose, hemicellulose, and lignin as well as a porous and irregular surface that enhances its adsorption capacity.

Kinetic studies indicated that the Pb (II) adsorption process is relatively fast, reaching equilibrium within approximately 30 min. Among the tested models, the Elovich model showed the best fit, suggesting a possible chemisorption. The Boyd model indicated that the rate-limiting step is governed by external (film) diffusion.

The equilibrium data were best described by the Sips isotherm model, which is consistent with the observed surface heterogeneity. Thermodynamic analysis revealed that the adsorption process is spontaneous, endothermic, and accompanied by increased system disorder, with characteristics compatible with physisorption.

Overall, SST biomass proved to be a promising, sustainable, and low-cost material for the removal of toxic metals from contaminated water, contributing to the advancement of environmentally friendly technologies and supporting circular economy practices in effluent treatment.

Acknowledgments

This research was supported by the Fundação Cearense de Apoio ao Desenvolvimento Científico e Tecnológico Grant N° BP5–0197–00133.01.00/22 and the Conselho Nacional de Desenvolvimento Científico e Tecnológico – CNPq Grants N° 409,820/2023 – 7 and N° 316,615/2023–4. The authors would like to thank also the financial support provided by the Coordination for the Improvement of Higher Education Personnel - Brazil (CAPES) and the Funding Authority for Studies and Projects - Brazil (FINEP). This article is a contribution of the National Institute of Science and Technology of the Health Economic-Industrial Complex (iCEIS) that supported this work.

The Article Processing Charge for the publication of this research was funded by the Coordenacao de Aperfeicoamento de Pessoal de Nivel Superior - Brasil (CAPES) (ROR identifier: 00x0ma614).

Conflict of Interests

The authors declare no conflict of interest.

Data Availability Statement

The data that support the findings of this study are available from the corresponding author upon reasonable request.

Keywords: Batch · Biosorption · Lead · *Spondias tuberosa*

[1] S. Pooja, D. Deblina, U. Aswathy, K. N. Ashok, S. L. Su, K. Sunil, *Environmental Pollution.* **2022**, *305*, 119248–119279.
[2] J. M. Reis, A. B. S. Aguiar, G. Freitas, V. C. Vassoler, G. V. L. Barros, G. E. Santos, I. Ramirez, R. P. Rodriguez, *Research, Society, and Development* **2022**, *11*, e5251126100.
[3] M. R. Awual, *J. Mol. Liq.* **2019**, *284*, 502–510.
[4] D. D. Giri, A. Alhazmi, A. Mohammad, S. Haque, N. Srivastava, V. K. Thakur, V. K. Gupta, D. B. Pal, *Chemosphere* **2022**, *287*, 132016.
[5] C. F. Carolin, P. S. Kumar, A. Saravanan, G. J. Joshiba, M. Naushad, *J. Environ. Chem. Eng.* **2017**, *5*, 2782–2799.
[6] A. El Mouden, N. El Messaoudi, A. El Guerraf, A. Bouich, V. Mehmeti, A. Lacherai, A. Jada, J. H. Pinê Américo-Pinheiro, *Environ. Res.* **2023**, *225*, 115606.
[7] Z. M. Şenol, E. Elma, N. El Messaoudi, V. Mehmeti, *J. Mol. Liq.* **2023**, *391*, 123310.
[8] S. Ghosh, A. Benettayeb, M. Meskini, B. Lal, Z. T. Al-Sharify, O. J. Ajala, A. Hosseini-Bandegharaei, *Environ. Technol. Rev.* **2024**, *13*, 359–378.
[9] M. Malbenia John, A. Benettayeb, M. Belkacem, C. R. Mitchel, M. H. Brahim, I. Benettayeb, B. Haddou, S. Al-Farraj, A. Ali Alkahtane, S. Ghosh, C. H. Chia, M. Sillanpaa, O. Baigenzhenov, A. Hosseini-Bandegharaei, *Chemosphere* **2024**, *357*, 142051..
[10] K. Oussadi, S. Al-Farraj, B. Benabdallah, A. Benettayeb, B. Haddou, M. Sillanpaa, *Biomass Conv. Bioref.* **2025**, *15*, 4803–4817.
[11] P. SenthilKumar, S. Ramalingam, V. Sathyaselvabala, S. D. Kirupha, S. Sivanesan, *Dessalinização* **2011**, *266*, 63–71.
[12] J. M. C. Meneses, A. M. da Silva Bento, J. H. da Silva, de Paula Filho FJ, J. G. M. da Costa, H. D. M. Coutinho, R. N. Pereira Teixeira, *Chemosphere* **2020**, *261*, 128144.
[13] W. D. Costa, W. Davi Costa, A. M. da Silva Bento, J. A. S. de Araújo, J. M. C. Menezes, J. G. M. da Costa, F. A. B. da Cunha, H. D. M. Coutinho, F. J. de Paula Filho, R. N. P. Teixeira, *Environ. Res.*, *183*, **2020**. 109213.
[14] A. Forgionny, N. Y. Acelas, R. Ocampo-Pérez, E. Padilla-Ortega, R. Leyva-Ramos, E. Flórez, *Environ. Sci. Pollut. Res.* **2021**, *28*, 23204–23219.
[15] H. J. Shamkhi, T. K. Hussein, *Journal of Ecological Engineering* **2022**, *23*, 158–168.

© 2025 The Author(s). *ChemistrySelect* published by Wiley-VCH GmbH.

[16] J. R. Regalbuto, J. Robles, *The engineering of Pt/Carbon Catalyst Preparation*, University of Illinois, Chicago **2004**.
[17] M. D. Granado-Castro, M. D. Galindo-Riaño, J. Gestoso-Rojas, L. Sánchez-Ponce, M. J. Casanueva-Marenco, M. Díaz-de-Alba, *Agronomy* **2024**, *14*, 554.
[18] L. D. Hafshejani, S. B. Nasab, R. M. Gholami, M. Moradzadeh, Z. Izadpanah, S. B. Hafshejani, A. Bhatnagar, *J. Mol. Liq.* **2015**, *211*, 448–456.
[19] Y. Tatiane da Costa Santos, G. Pereira da Costa, J. Marcell Coelho Menezes, J. Victor Serra Nunes, A. Hosseini-Bandegharaei, H. Douglas Melo Coutinho, D. Sena Júnior, F. José de Paula Filho, R. Nonato Pereira Teixeira, *Results in Chem.* **2024**, *7*, 101339,
[20] L. C. N. Iha, O. L. M. Cruz, *Brazilian Journal of Otorhinolaryngology* **2020**, *86*, 222–227.
[21] J. V. I. MOREIRA, et al., *Revista Virtual de Química* **2019**, *11*, 237–254.
[22] J. D. S. Silva, R. D. S. Barros, L. D. O. Cruz, L. D. O. Cruz, F. N. Ani, M. D. F. Salgado, Produção de carvão ativado da casca do babaçu e sua eficiência no tratamento de água para o consumo humano, in: Engenharia Florestal: Desafios, Limites e Potencialidade, Editora Científica Digital, Guarujá, SP, **2020**, pp. 654–685.
[23] K. A. M. Salih, K. G. Zhou, E. Guibal, E. A. Basiony, L. A. Nassar, A. A. H. Abdel-Rahman, M. F. Hamza, *Chem. Eng. J.* **2025**, *505*, 159469.
[24] G. E. Acquah, B. K. Via, O. O. Fasina, L. G. Eckhardt, *J. Anal. Methods Chem.* **2016**, *2016*, 28003929.
[25] J. B. Neris, F. H. M. Luzardo, E. G. P. da Silva, F. G. Velasco, *Chem. Eng. J.* **2019**, *357*, 404–420.
[26] R. Javier-Astete, J. Jimenez-Davalos, G. Zolla, *PLoS One* **2021**, *16*, https://doi.org/10.1371/journal.pone.0256559.
[27] S. I. Mohammadabadi, V. Javanbakht, *Intern. Jour. of Biolog. Macromol.* **2020**, *164*, 1133–1148.
[28] J. Zolgharnein, S. D. Farahani, *J. Chemom.* **2023**, *37*, e3396.
[29] N. Khan, F. Wahid, Q. Sultana, N. U.s Saqib, M. Rahim, *SN Appl. Sci.* **2020**, *2*, 753.
[30] J. Cruz Olivares, C. Pérez-Alonso, C. Barrera-Díaz, R. Natividad, M.C. Chaparro-Mercado, *Chem. Eng. J.* **2011**, *166*, 814–821.
[31] M. I. El-Khaiary, G. F. Malash, *Hydrometallurgy* **2011**, *105*, 314–320.
[32] E. C. Lima, M. H. Dehghani, A. Guleria, F. Sher, R. R. Karri, G. L. Dotto, H. N. Tran, in *Green Technologies for Defluorination of Water* (Eds: M. H. Dehghani, R. R. Karri, E. C. Lima), Elsevier, Amsterdan, Netherlands **2021**, Chapter 3, pp. 41–88.
[33] M. Aguareles, E. Barrabés, T. Myers, A. Valverde, *Physica D: Nonlinear Phenomena* **2023**, *448*, 133690.
[34] R. Sips, *J. Chem. Phys.* **1948**, *16*, 490–495.
[35] L. L. Pérez Antolinez, I. C. Paz Astudillo, A. P. Sandoval Aldana, G. C. Peñaloza Atuesta, *Revista EIA* **2020**, *17*, 1–13.
[36] J. M. C. Menezes, A. M. da Silva Bento, F. J. de Paula Filho, J. G. M. da Costa, H. D. M. Coutinho, R. N. P. Teixeira, *Sustain. Chem. Pharm.* **2021**, *19*, 100364.
[37] Y. Santos, G. Costa, J. Menezes, A. Feitosa, H. Coutinho, D. Sena Jr., F. Filho, R. Teixeira, *Int. J. Environ. Res. Public Health* **2022**, *19*, 16283.
[38] E. C. Lima, A. Hosseini-Bandegharaei, J. C. Moreno-Piraján, I. Anastopoulos, *J. Mol. Liq.* **2019**, *273*, 425–434.
[39] G. Ozsin, M. Kılıç, E. Apaydın-Varol, *Applied Water Science* **2019**, *9*, 2–14.
[40] N. Erdol-Aydin, S. Sezer, B. Esin, G. Nasun-Saygili, *Adsorpt. Sci. Technol.* **2024**, 42, https://10.1177/02636174241266707.
[41] A. Fenti, P. Iovino, S. Salvestrini, *J. Mol. Liq.* **2019**, *273*, 425–434.
[42] R. F. do Nascimento, A. C. A. de Lima, C. B. Vidal, D. de Quadros Melo, G. S. C. Raulino, *Adsorção: aspectos teóricos e aplicações ambientais*, 1st ed, Imprensa Universitária, Universidade Federal do Ceará, Fortaleza, **2014**, p. 256.
[43] M. Azadian, H. Ghanadzadeh Gilani, H. Rajabi-Kuyakhi, N. Gharibipour, *Environ. Prog. Sustainable Energy* **2022**, *41*, e13751.
[44] S. Hasanzadeh, S. Mortazavi-Derazkola, R. Khosravi, *Desalination and Water Treatment* **2024**, *318*, 100347.

Manuscript received: April 17, 2025

© 2025 The Author(s). *ChemistrySelect* published by Wiley-VCH GmbH.